Radiomics Feature Analysis Using Native T1 Mapping for Discriminating Between Cardiac Tumors and Thrombi

Jinwoo Son, MD, Yoo Jin Hong, MD, PhD, Sujeong Kim, MS, Kyunghwa Han, PhD, Hye-Jeong Lee, MD, PhD, Jin Hur, MD, PhD, Young Jin Kim, MD, PhD, Byoung Wook Choi, MD, PhD

Rationale and Objectives: Accurate differential diagnosis is essential because cardiac tumors and thrombi have different prognoses and therapeutic approaches. Native T1 map provides an objective T1 time quantifications of cardiac mass without the need for a contrast agent. We examined the diagnostic performance of radiomics features for differentiating cardiac tumors from thrombi using cardiac magnetic resonance imaging T1 mapping technique compared to that of late gadolinium enhancement (LGE) imaging.

Materials and Methods: This retrospective study included 22 cardiac tumors and 21 thrombi of 41 patients who underwent cardiac magnetic resonance imaging from December 2013 to May 2018. Fifty-six radiomics features were extracted from native T1 images. The least absolute shrinkage and selection operator method was used for feature selection and rad score extraction. The diagnostic performance of the rad score was compared to that of the native T1 value (mean T1) and LGE ratio.

Results: The area under the receiver operating characteristic curve of the rad score was higher than that of the mean T1 and LGE ratio (0.98 vs. 0.86 vs. 0.82, $p = 0.001$). With the optimal cut-off value, the rad score showed sensitivity, specificity, and accuracy of 95.4%, 95.2%, and 95.2%, respectively. Combination of the rad score and mean T1 showed a significantly higher diagnostic performance than mean T1 ($p = 0.019$) or LGE ratio ($p = 0.022$).

Conclusion: The rad score derived from native T1 maps can differentiate thrombi from tumors better than the mean T1 or LGE ratio. This is valuable for determining a treatment strategy for cardiac lesions in patients who cannot tolerate contrast agents.

Key Words: Radiomics; Native T1 mapping; Cardiac tumors; Cardiac thrombi; Late gadolinium enhancement.

Abbreviations: MRI magnetic resonance imaging, **LGE** late gadolinium enhancement, **GLRLM** gray-level run length matrix, **LASSO** least absolute shrinkage and selection operator, **ROC** receiver operating characteristic, **AUC** area under the ROC curve, **ICC** intraclass correlation coefficient

INTRODUCTION

Cardiac tumors are rare, with a reported prevalence rate of less than 1% (1–3). The treatment of choice for cardiac tumors is surgical resection (1). Cardiac thrombi have a prevalence higher than that of cardiac tumors (2,4) and require prompt anticoagulation treatment. Because the therapeutic approaches are different depending on the diagnosis, accurate differentiation between these two diseases is essential (2). Although several studies have investigated methods for distinguishing cardiac tumors from thrombi using various imaging tools, including echocardiography, cardiac computed tomography (CT), or magnetic resonance imaging (MRI) (5–8), differentiation remains challenging. Cardiac MRI is a useful tool for differential diagnosis of cardiac masses because of its good tissue characterization (2,9). Cardiac thrombi have a similar appearance with cardiac tumors, and the T1- and T2-weighted signals vary depending on the age of a thrombus, making differential diagnosis difficult (10). Previous studies have used many features, such as signal intensity on gradient echo sequence or degree of gadolinium enhancement, both of which are influenced by the image acquisition protocol

Acad Radiol 2022; 29:S1–S8

From the Department of Radiology and Research Institute of Radiological Science, Severance Hospital, Yonsei University College of Medicine, 50 Yonsei-ro, Seodaemun-gu, Seoul 120-752, South Korea (J.S., Y.J.H., K.H., H.-J.L., J.H., Y.J.K., B.W.C.); Departments of Biostatistics and Computing, Yonsei University Graduate School, Seoul, South Korea (S.K.). Received June 23, 2020; revised December 6, 2020; accepted December 17, 2020. **Address correspondence to:** Y.J.H. e-mail: uzzin@yuhs.ac

https://doi.org/10.1016/j.acra.2020.12.009

and the reader's subjectivity (2,11–14). Late gadolinium enhancement (LGE) MRI is one of the established methods for differentiation of cardiac tumors and thrombi; however, it requires contrast agents (15,16).

Native T1 mapping is a promising MRI technique that allows quantitative analysis of the true relaxation time of each voxel without a contrast agent (17). Due to these properties, it has been evaluated as a means to characterize cardiac tumors (18,19). Nevertheless, the differentiation of cardiac tumors and thrombi by MRI remains arduous.

The emergence of radiomics has enabled a more objective image analysis. It involves transforming image data into computer-based, high-dimensional data. These quantitative data can provide more information on the tissue characteristics than visual assessment (20). Several recent studies using the radiomics approach conducted in various cardiac diseases revealed its potential usefulness (21–26).

Since cardiac tumors and thrombi differ in their tissue composition, we hypothesized that radiomics features from native T1 maps could be potentially useful tools for discriminating between cardiac tumors and thrombi. Therefore, the purpose of this study was to investigate the diagnostic performance of radiomics analysis using native T1 maps for distinguishing cardiac tumors from thrombi.

MATERIALS AND METHODS

Ethical Considerations

This retrospective study was approved by the Institutional Review Board of our center (approval number: 4-2019-0838). The requirement for written informed consent was waived.

Patient Selection

By review of medical and radiologic records dated from December 2013 to May 2019, we identified 51 consecutive patients who underwent cardiac MRI for the evaluation of a cardiac mass. Extracardiac masses ($n = 5$) and cardiac tumors with dense calcification ($n = 1$) or a lipid component ($n = 4$) were excluded. Finally, 43 lesions from 41 patients were included for analysis. These included 22 tumors from 22 patients and 21 thrombi from 19 patients. Three thrombi were found in one patient. Tumors were diagnosed clinically or based on pathologic reports ($n = 13$). Clinical diagnosis was based on the clinical information and follow-up imaging studies (median follow-up period: 6 months, range 4–21 months) including cardiac MRI ($n = 1$), CT ($n = 4$) and echocardiography ($n = 4$). These included the following final diagnosis: sarcoma ($n = 7$), myxoma ($n = 4$), cavernous hemangioma ($n = 3$), metastasis ($n = 3$), papillary fibroelastoma ($n = 2$), paraganglioma ($n = 2$), fibroma ($n = 1$). Thrombi were diagnosed based on the patient's response to anticoagulation treatment. All thrombi were reduced in size ($n = 6$) or had completely disappeared ($n = 14$) on follow-up echocardiography. One thrombus was pathologically confirmed.

Cardiac MRI Protocol

MRI was performed on a 3.0-T scanner (Magnetom Trio Tim; Siemens AG Healthcare Sector, Erlangen, Germany) with a six-element body matrix coil and a spine matrix coil array. Native T1 mapping was performed using a modified Look-Locker inversion-recovery sequence with 5(3)3 protocol at end-expiration in a plane covering the largest diameter of the cardiac mass. We employed the nonselective inversion pulse True FISP single-shot readout sequence in the mid-diastolic phase, with the following parameters: field of view, 306 × 360 mm; acquisition matrix, 144 × 256; slice thickness, 8 mm; TR, 2.24 ms; TE, 1.12 ms; minimum inversion time, 100 ms; inversion time increment, 80 ms; flip angle, 35°; parallel acquisition technique factor, 2; number of inversions, 3. Five images were acquired after the first inversion; following a pause for three heart beats, three images were acquired after the second inversion. Fully automated nonrigid motion correction was applied to register the individual TI images before inline T1 fitting was performed using a monoexponential three-parameter fit. LGE MRI was performed 10 min (mean ± standard deviation: 9.68 ± 2.21 min) after contrast agent injection (0.2 mmol/kg; Dotarem; Guerbet, Villepinte, France) using a magnitude- and phase-sensitive inversion recovery–prepared True FISP sequence (typical TR/TE, 5.83/3.24 ms; flip angle, 15°; slice thickness, 8 mm; field of view, 380 mm; matrix, 320 × 320 pixels; number of signal average, 2).

Lesions Characteristics and Quantitative Image Analysis

Two radiologists (Y.J.H., J.W.S.) with 12 and 3 years of experience in cardiac MRI, respectively, were blinded to the final pathological results and reviewed all images. They recorded the number, size, and location of all masses observed on the MR images by consensus. For quantitative analysis of the T1 map images, regions of interest (ROIs) covering the entire cardiac mass were drawn manually by one radiologist (J.W.S.) and confirmed by the other radiologist (Y.J.H.). Figure 1 shows examples of segmentation. For quantitative analysis of the LGE images, the ROIs covering the cardiac masses and normal myocardium on the representative magnitude image covered the largest diameter of the lesion. The mean signal intensity of the normal myocardium and cardiac lesions was recorded. The signal intensity ratios (LGE ratios) were calculated as follows (15):

$$\text{LGE ratio} = \text{Signal intensity of lesion}/\text{Signal intensity of myocardium}$$

Radiomics Feature Extraction

Radiomics feature extraction from the T1 map images was performed using commercial software (AVIEW; Coreline Soft, Seoul, Republic of Korea) based on the segmented ROIs on the T1 maps. In the feature extraction, the value

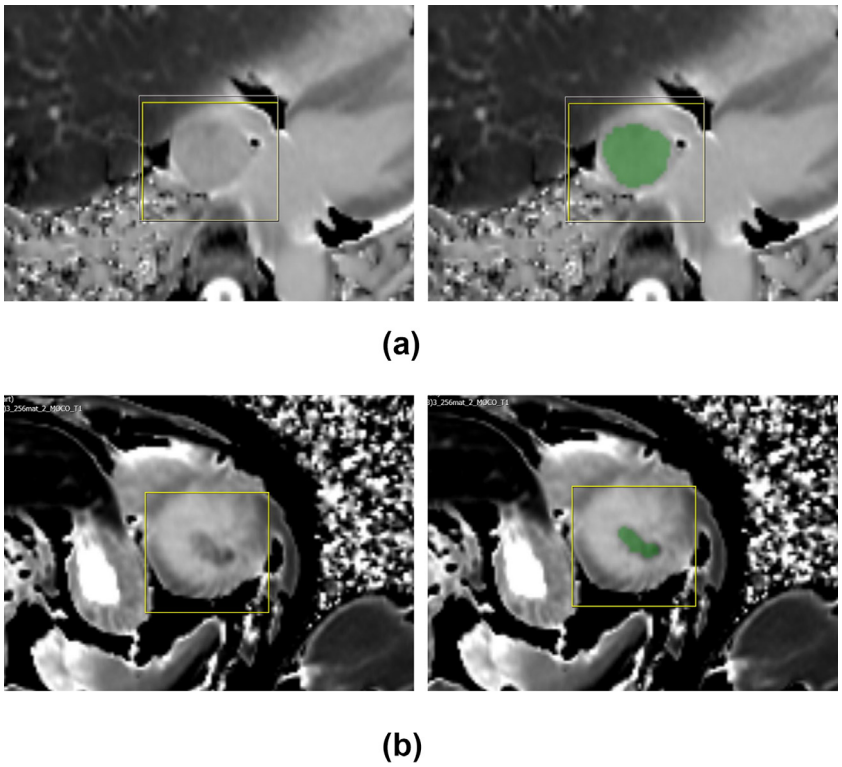

Figure 1. Segmentation example. (a) Images obtained from a 56-year-old woman with no other relevant history. The lesion was located in the right atrium and had a diameter of 17 × 15 mm. The patient underwent surgery for cardiac mass excision. The lesion was pathologically confirmed as a cavernous hemangioma. (b) Images obtained from a 50-year-old man with a history of dilated cardiomyopathy and arrhythmia. The lesion was located in the left ventricle and had a diameter of 14 × 11 mm. The lesion completely disappeared on the follow-up echocardiography after 1 month.

range was set to 0−3000 and the bins value to 128. A total of 56 radiomics features were obtained: 10 histogram, 6 percentile, 2 gradient, 13 gray-level co-occurrence matrix, 13 gray-level run length matrix, two moment, one fractal, and nine shape features. The specific features contained in each class are described in Supplementary Table E1. The extracted radiomics features of each lesion were recorded. The same measurement was repeated after 3 weeks, and intraobserver reproducibility for radiomics features was assessed.

We additionally drew an ROI on a focal area of the ventricular septum to validate the reproducibility of the radiomics feature extraction (27). The mean, minimum, maximum and standard deviation of the native T1 values measured from the same area were compared to the first-order statistics obtained by radiomics feature extraction.

Radiomics Feature Selection and Rad Score Extraction

The least absolute shrinkage and selection operator approach was used to select the significant radiomics features and to build a classification model. Ten-fold cross-validation with 100 repetitions was performed. Feature selection was made based on the relative standard deviation of each feature's coefficients. Each coefficient was an average value of 100 repetitions. The selected features were extracted, and their linear combination formed the rad score of each lesion. Feature selection and modelling were performed using R software (version 3.5.1;R foundation, Vienna, Austria) and "glmnet" package (version 2.0-16) (28).

Statistical Analysis

Categorical variables were compared using Pearson's chi-square test or Fisher's exact test. Continuous variables were compared using Mann-Whitney's *U* test. Optimal cut-off values for rad score, mean T1, and LGE ratio were determined using Youden's index (29). Diagnostic performances were evaluated based on the receiver operating characteristic (ROC) curves and areas under the ROC curve (AUCs) using the bootstrap method. The comparisons between ROC curves were performed using the bootstrap method. All bootstrap methods used 1000-time resampling. Intraobserver reproducibility was assessed by intraclass correlation coefficients (ICCs), and features with low reproducibility (ICC <0.75) were excluded from analysis (23). The reproducibility of radiomics feature extraction was evaluated by Lin's concordance correlation coefficients. A two-sided $p < 0.05$ was considered to indicate a statistically significant difference. All statistical analyses were performed using R software (version 3.6; R Foundation for Statistical Computing).

RESULTS

Patients' and Lesions' Characteristics

Figure 2 shows the flow of the patient selection process and Table 1 shows the patients' characteristics. Age was significantly higher in the tumor group ($p < 0.001$). The location of the lesions also showed a significant difference ($p < 0.001$). Of the 22 tumors, seven were located in the left atrium, three in the left ventricle, three in the right ventricular outflow tract, five in the right atrium, and four in the right ventricle.

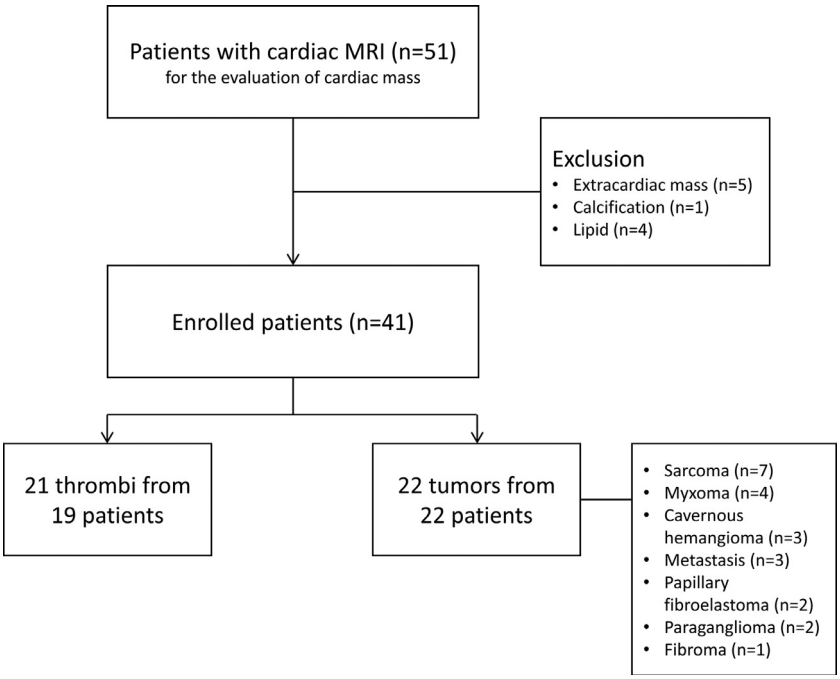

Figure 2. The flow diagram of the patient selection process.

Of the 21 thrombi, 18 were located in the left ventricle, two in the right atrium, and one in the right ventricle. Lesions were significantly larger in the tumor group ($p < 0.001$).

Thrombi were classified as either protruding (the free margin of the lesion was concave following the curvature of the endocardial surface) or mural (the free margin was convex in relation to the adjacent endocardium) based on their shape (30). Of the total 21 thrombi, 17 (81 %) were protruding, and 4 (19 %) were murals. Thrombi were also classified according to the onset of symptoms as recent (less than 1 month) and old (more than 1 month) (19,31). Seventeen thrombi (81 %) were recent and four (19 %) were old.

TABLE 1. Patients' Characteristics

Patients' Characteristics			
	Tumor ($n = 22$)	Thrombus ($n = 19$)	p Value
Sex	M = 12, F = 10	M = 15, F = 4	0.128
Age; mean ± SD (range)	63.0 ± 11.8 (30−78)	50.6 ± 13.9 (21−75)	<0.001
DM	3	5	0.457
HTN	10	4	0.104
Smoking	6	9	0.452
Hyperlipidaemia	4	1	0.345
Prior CVA/TIA	1	3	0.345
Heart disease*	4	9	0.063
Arrhythmia	2	3	0.664
Lesion characteristics			
	Tumor ($n = 22$)	Thrombus ($n = 21$)	p Value
Location	7 LA, 3 LV, 3 RVOT, 5 RA, 4 RV	18 LV, 2 RA, 1 RV	<0.001
Size (long); mean ± SD (mm)	38.1 ± 19.0	20.6 ± 9.6	<0.001
Size (short); mean ± SD (mm)	28.3 ± 15.7	10.7 ± 3.8	<0.001
Classification of thrombi		17 protruding, 4 mural	
Age of thrombi		17 recent, 4 old	

CVA, cerebrovascular accident; DM, diabetes mellitus; HTN, hypertension; LA, left atrium; LV, left ventricle; RA, right atrium; RV, right ventricle; RVOT, right ventricular outflow tract; SD, standard deviation; TIA, transient ischaemic attack.

Patients' age and lesion size are presented as the mean value ± standard deviation with the minimum and maximum values in parentheses. p values were calculated using Mann-Whitney's U test for continuous data and Pearson's chi-square test or Fisher's exact test for categorical data.

* 1 with aortic regurgitation and 3 with coronary artery disease in the tumor group, 4 with dilated cardiomyopathy, 1 with hypertrophic cardiomyopathy, and 4 with coronary artery disease in the thrombus group.**The final diagnoses of the tumors were as follows: 7 sarcomas, 3 cavernous haemangiomas, 3 metastases, 1 fibroma, 4 myxomas, 2 papillary fibroelastomas, and 2 paragangliomas.

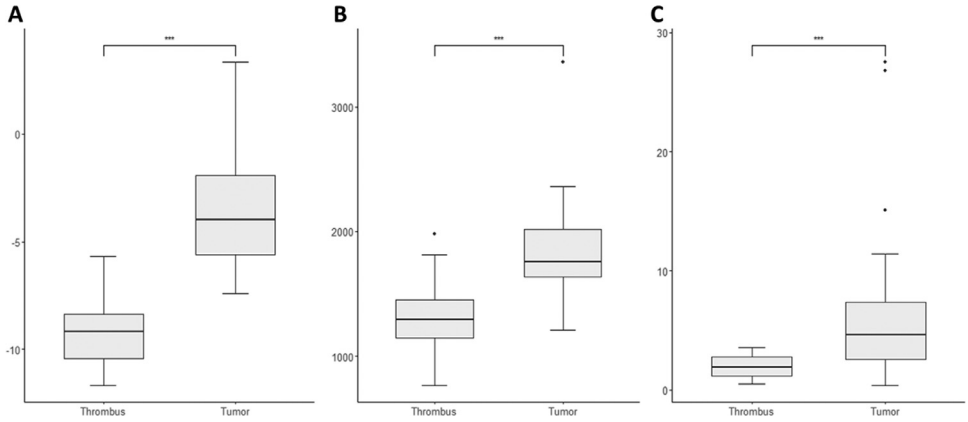

Figure 3. Box-and-whisker plots showing the tumor and thrombus (a) rad score, (b) mean T1, and (**c**) late gadolinium enhancement ratio. The center line in each box represents the median. The lower and upper limits of each box represent the 25th and 75th percentile, respectively. Whiskers extend to the most extreme observations within the 25th and 75th percentiles ± 1.5 × interquartile range. Observations outside the whiskers are shown as dots.

Reproducibility of Radiomics Data Acquisition

The first-order radiomics features extracted from an ROI on the interventricular septum were compared to native T1 value measurements from the same region. The Lin's concordance correlation coefficients of mean, minimum, maximum, and standard deviation were 0.994, 0.992, 0.986, and 0.997, respectively, which indicates substantial to almost perfect agreement (32).

Mean T1 and LGE Ratio

Tumors had significantly higher mean T1 values and LGE ratios than did thrombi (1843.8 ± 493.0 vs. 1246.2 ± 364.3, $p < 0.001$ and 7.1 ± 7.4 vs. 2.0 ± 1.0, $p < 0.001$, respectively). Figure 3 shows the distribution of mean T1 values and LGE ratios of the tumors and thrombi.

Radiomics Feature Selection and Rad Score Extraction

Seven of the 56 features were excluded due to a lack of intra-observer reproducibility (ICC < 0.75). The excluded features were excess-kurtosis, skewness, and five gray-level run length matrix features (gray-level nonuniformity, high gray-level run emphasis, run length nonuniformity, short run emphasis, and short run high gray-level emphasis). Finally, 49 features were included in the analysis. Based on the least absolute shrinkage and selection operator method, 6 of the 49 features were selected as follows: (1) orthogonal axis, (2) max, (3) roundness, (4) percentile_10, (5) fractal dimension, and (6) percentile_25. The rad score was calculated with the following equation:

$$\text{Rad score} = -21.02 + 0.13 \times \text{orthogonal axis} + 0.002 \times \text{max} + 6.34 \times \text{roundness} + 0.001 \times \text{percentile\_10} + 1.89 \times \text{fractal dimension} + 0.001 \times \text{percentile\_25}$$

Figure 3 shows the rad score distribution. There was a significant difference in the rad score between thrombi and tumors ($p < 0.001$).

Diagnostic Performances of the Rad Score, Mean T1, and LGE Ratio

The diagnostic performances of the rad score, mean T1, LGE ratio, and their combinations are summarised in Table 2. Comparisons of the ROC curves of these models are shown in Figure 4. The rad score demonstrated excellent diagnostic performance with an AUC of 0.98. With a cut-off value of −6.5, it demonstrated sensitivity, specificity, and diagnostic accuracy of 95.4%, 95.2%, and 95.4%, respectively. The mean T1 demonstrated a lower diagnostic performance (AUC: 0.86) than that of the rad score. With a cut-off value of 1540.3 ms, it showed sensitivity, specificity, and accuracy of 81.8%, 81.0%, and 81.4%, respectively. The LGE ratio also demonstrated a lower diagnostic performance than that of the rad score (AUC: 0.82). With a cut-off value of 3.4, it showed sensitivity, specificity, and accuracy of 68.2%, 95.2%, and 81.4%, respectively.

The combination of rad score and mean T1 yielded an AUC of 0.98. If the criterion is set to satisfy only one of the cut-off values of the rad score and the mean T1, the sensitivity is 100%, specificity is 81.0%, and accuracy is 90.7%. If the criterion is set to satisfy both cut-offs, the sensitivity is 77.3%, specificity is 95.2%, and accuracy is 86.1%. The combination model demonstrated a significantly higher AUC value compared to those of the mean T1 ($p = 0.019$) or LGE ratio alone ($p = 0.022$).

DISCUSSION

Here, we evaluated the diagnostic performance of the rad score derived from native T1 maps to distinguish cardiac tumors from thrombi. The rad scores of cardiac tumors and thrombi were significantly different. The rad score alone and the combination model with the mean T1 demonstrated a higher diagnostic ability than did the mean T1 or LGE ratio alone. This small proof of concept study showed that native T1 maps and radiomics analysis can differentiate cardiac

TABLE 2. Cut-off Values and Diagnostic Performances of the Rad Score, Mean T1, and LGE Ratio

	Cut-off Value	Sensitivity (%)	Specificity (%)	Accuracy (%)	AUC	Comparison with "Rad Score + Mean T1" (*p* Value)
Individual						
Rad score	-6.5	95.4 (77.2, 99.9)	95.2 (76.2, 99.9)	95.4 (84.2, 99.4)	0.98 (0.95, 1)	>0.99
Mean T1	1540.3 ms	81.8 (59.7, 94.8)	81.0 (58.1, 94.6)	81.4 (66.6, 91.6)	0.86 (0.74, 0.97)	0.019
LGE ratio	3.4	68.2 (45.1,86.1)	95.2 (76.2, 99.9)	81.4 (66.6, 91.6)	0.82 (0.69, 0.95)	0.022
Combination						
Rad score + mean T1	OR*	100.0 (84.6, 100)	81.0 (58.1, 94.6)	90.7 (77.9, 97.4)	0.98 (0.96, 1)	
	AND**	77.3 (54.6, 92.2)	95.2 (76.2, 99.9)	86.1 (72.1, 94.7)		

AUC, area under the receiver operating characteristic curve; LGE, late gadolinium enhancement.

Comparison between the two diagnostic models was made using the bootstrap method. The 95% confidence intervals are shown in parentheses.

* Rad score ≥ −6.5 or mean T1 ≥ 1540.3 ms.

** Rad score ≥ −6.5 and mean T1 ≥ 1540.3 ms.

tumors from thrombi with high accuracy and without the use of contrast agents.

We found six radiomics features with the best discrimination between cardiac thrombi and tumors. Of these, the orthogonal axis, the longest distance in a straight line perpendicular to the longest axis, was larger in tumors. Similarly, roundness was higher in tumors than in thrombi. The rounder the shape, the greater the likelihood the mass was a tumor rather than a thrombus, which is consistent with some previous reports (33−35). Furthermore, the maximum T1 value, percentile_10, and percentile_25 (i.e., percentile values that correspond to the bottom 10% and 25% of the T1 value, respectively) were higher in cardiac tumors. In the previous study, tumors generally had a longer T1 relaxation time than thrombi, although there was no significant difference (19). We demonstrated that not only the mean T1, but the maximum and bottom 10% and 25% of the T1 values are also useful for differentiation between cardiac tumors and thrombi. Of the thrombi included in this study, 81% were protruding, and recent. These thrombi have a relatively round shape and a relatively high T1 signal intensity, making it difficult to differentiate them from tumor (19). Nevertheless, this study revealed that these factors differ between thrombi and tumors with quantification by radiomics analysis. Additionally, fractal dimension is associated with the complexity and homogeneity of the structure (36). In this study, its value was higher in the tumor than in the thrombus, indicating a more complex structure in the tumor. In summary, based on the selected radiomics features, the larger, rounder, and more complex the lesion and the longer its T1 relaxation time, the more likely it is a tumor rather than a thrombus.

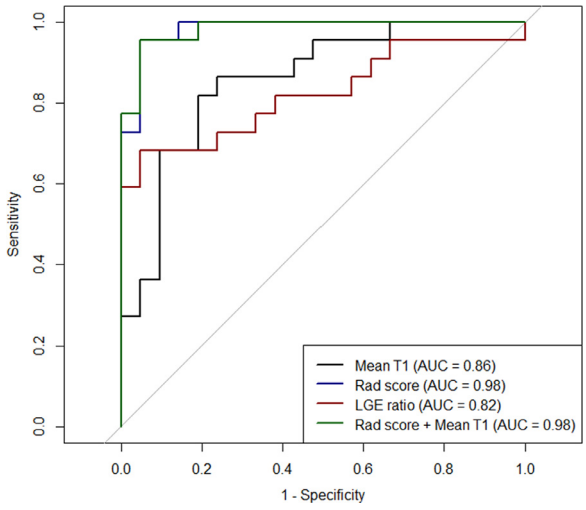

Figure 4. Comparison of the receiver operating characteristic curve among the models. The rad score + mean T1 showed significantly higher AUC values compared to those of the mean T1 alone ($p = 0.019$) or LGE ratio ($p = 0.022$). AUC, area under the receiver operating characteristic curve; LGE, late gadolinium enhancement.

Native T1 and T2 mapping has made great strides in the diagnosis of myocardial disease. Several small observational studies and case reports have analyzed cardiac tumors and thrombi using T1 and T2 mapping. However, these studies did not prove that cardiac tumors and thrombi can be discriminated with native T1 and T2 relaxation times (18,19,37,38). In our study, the mean native T1 values were significantly different between tumors and thrombi, possibly due to the composition of the tumor group. We included only solid tumors because it is challenging to differentiate them from thrombi (39,40). Tumors with cysts, calcification, or lipids, which may have characteristic features on CT or other modalities, were excluded.

Native T1 mapping has many strengths in radiomics analysis. Due to variation in the signal intensity between intra-scan or inter-scan images, signal intensity normalization should be applied prior to quantitative texture analysis of MR images (41). However, in T1 maps, every pixel in the map represents the objective corresponding T1 values of cardiac masses under the same scanning conditions (42). Thus, T1 maps do not require complex pre-processing steps, such as normalization or inhomogeneity correction, improving reproducibility in radiomics analysis. Recently, it has been reported that

radiomics analysis using native T1 or T2 maps can be useful in the diagnosis of various cardiac diseases. Neisius et al. (21) demonstrated the possibility of distinguishing hypertensive heart disease from hypertrophic cardiomyopathy using a radiomics feature obtained from a T1 map of the myocardium. They showed that radiomics had a higher accuracy than that of the global native T1 value. Baessler et al. (26) reported that texture analysis of T1 and T2 maps had high accuracy for diagnosing acute infarct-like myocarditis. Radiomics yielded better diagnostic performance than that of clinical criteria or global myocardial T1 and T2 values.

LGE cardiovascular MRI has shown a higher diagnostic value for distinguishing cardiac tumors from thrombi compared to other modalities (15,16,43). However, its scope is limited by the need for contrast agents and the delay between contrast injection and image acquisition. Native T1 mapping does not require contrast agents. Therefore, radiomics analysis using native T1 maps can be an alternative to LGE MRI in patients with chronic kidney disease, in whom gadolinium administration should be avoided.

This study has several limitations. First, the major limitation of this study is the small sample size. Hence, the radiomics model of this study was not verified in an independent validation set. Due to this, the model may be overfitted to the small population included in this study. This is an inevitable limitation resulting from the rarity of cardiac tumors. To overcome this limitation, the diagnostic performance was evaluated using a bootstrap resampling method to secure the validity and reproducibility of the results. This pilot study explored the possibility of radiomics analysis using native T1 map to differentiate cardiac tumor from thrombus. However, a further study with a larger sample size is required to validate the present results. Second, there were inherent limitations to the retrospective study design. Third, tumor pathology was heterogeneous. Because cardiac tumors are rare, it was difficult to form a group with a single pathology for analysis (2). This limits the generalizability of the present study results and makes it difficult to apply the results to clinical practice. Thus, a future study is warranted, based on a single tumor pathology, to evaluate the feasibility of practical use of radiomics analysis in the differential diagnosis of cardiac masses. Fourth, some tumors in this study were not pathologically confirmed, and the diagnosis was based on a follow-up study. Fifth, perfusion images were not included in the analysis. Lastly, interobserver reproducibility was not evaluated. Instead, intraobserver reproducibility was verified to secure the reproducibility of the feature extraction.

CONCLUSIONS

Radiomics analysis using native T1 maps can differentiate cardiac tumors from thrombi with a higher accuracy than those of the mean T1 or LGE ratio, without requiring contrast agents. Hence, it may be useful for differentiating cardiac thrombi from tumors when other imaging modalities are inconclusive and gadolinium contrast imaging is not feasible.

FUNDING

This work was supported by the National Research Foundation of Korea (grant NRF-2017R1A2B4009661 and NRF-2020R1F1A1074983).

REFERENCES

1. Butany J, Nair V, Naseemuddin A, et al. Cardiac tumours: diagnosis and management. Lancet Oncol 2005; 6:219–228.
2. Pazos-Lopez P, Pozo E, Siqueira ME, et al. Value of CMR for the differential diagnosis of cardiac masses. JACC Cardiovasc Imaging 2014; 7:896–905.
3. McAllister Jr. HA, Hall RJ, Cooley DA. Tumors of the heart and pericardium. Curr Probl Cardiol 1999; 24:57–116.
4. Mollet NR, Dymarkowski S, Volders W, et al. Visualization of ventricular thrombi with contrast-enhanced magnetic resonance imaging in patients with ischemic heart disease. Circulation 2002; 106:2873–2876.
5. Gaibazzi N, Giumelli C, Martella EM, et al. Contrast-echocardiography for the differential diagnosis of atrial masses. Eur Heart J 2013; 34:1957.
6. Zaragoza-Macias E, Chen MA, Gill EA. Real time three-dimensional echocardiography evaluation of intracardiac masses. Echocardiography 2012; 29:207–219.
7. Hong YJ, Hur J, Kim YJ, et al. Dual-energy cardiac computed tomography for differentiating cardiac myxoma from thrombus. Int J Cardiovasc Imaging 2014; 30(Suppl 2):121–128.
8. Hong YJ, Hur J, Kim YJ, et al. The usefulness of delayed contrast-enhanced cardiovascular magnetic resonance imaging in differentiating cardiac tumors from thrombi in stroke patients. Int J Cardiovasc Imaging 2011; 27(Suppl 1):89–95.
9. Luna A, Ribes R, Caro P, et al. Evaluation of cardiac tumors with magnetic resonance imaging. Eur Radiol 2005; 15:1446–1455.
10. Motwani M, Kidambi A, Herzog BA, et al. MR imaging of cardiac tumors and masses: a review of methods and clinical applications. Radiology 2013; 268:26–43.
11. Semelka RC, Shoenut JP, Wilson ME, et al. Cardiac masses: signal intensity features on spin-echo, gradient-echo, gadolinium-enhanced spin-echo, and TurboFLASH images. J Magn Reson Imaging 1992; 2:415–420.
12. Seelos KC, Caputo GR, Carrol CL, et al. Cine gradient refocused echo (GRE) imaging of intravascular masses: differentiation between tumor and nontumor thrombus. J Comput Assist Tomogr 1992; 16:169–175.
13. Paydarfar D, Krieger D, Dib N, et al. In vivo magnetic resonance imaging and surgical histopathology of intracardiac masses: distinct features of subacute thrombi. Cardiology 2001; 95:40–47.
14. Buckley O, Madan R, Kwong R, et al. Cardiac masses, part 1: imaging strategies and technical considerations. AJR Am J Roentgenol 2011; 197:W837–W841.
15. Hong YJ, Hur J, Han K, et al. Quantitative analysis of a whole cardiac mass using dual-energy computed tomography: comparison with conventional computed tomography and magnetic resonance imaging. Sci Rep 2018; 8:15334.
16. Weinsaft JW, Kim HW, Shah DJ, et al. Detection of left ventricular thrombus by delayed-enhancement cardiovascular magnetic resonance prevalence and markers in patients with systolic dysfunction. J Am Coll Cardiol 2008; 52:148–157.
17. Germain P, Ghannudi SE, Jeung M-Y, et al. Native T1 mapping of the heart – a pictorial review. Clin Med Insights Cardiol 2014; 8s4:CMC.S19005.
18. Ferreira VM, Holloway CJ, Piechnik SK, et al. Is it really fat? Ask a T1-map. Eur Heart J Cardiovasc Imaging 2013; 14:1060.
19. Caspar T, El Ghannudi S, Ohana M, et al. Magnetic resonance evaluation of cardiac thrombi and masses by T1 and T2 mapping: an observational study. Int J Cardiovasc Imaging 2017; 33:551–559.
20. Gillies RJ, Kinahan PE, Hricak H. Radiomics: images are more than pictures, they are data. Radiology. 2016; 278:563–577.
21. Neisius U, El-Rewaidy H, Nakamori S, et al. Radiomic analysis of myocardial native t1 imaging discriminates between hypertensive heart disease and hypertrophic cardiomyopathy. JACC Cardiovasc Imaging 2019; 12:1946–1954.
22. Baessler B, Mannil M, Maintz D, et al. Texture analysis and machine learning of non-contrast T1-weighted MR images in patients with hypertrophic cardiomyopathy-preliminary results. Eur J Radiol 2018; 102:61–67.
23. Baessler B, Mannil M, Oebel S, et al. Subacute and chronic left ventricular myocardial scar: accuracy of texture analysis on nonenhanced cine MR images. Radiology 2018; 286:103–112.

24. Gibbs T, Villa ADM, Sammut E, et al. Quantitative assessment of myocardial scar heterogeneity using cardiovascular magnetic resonance texture analysis to risk stratify patients post-myocardial infarction. Clin Radiol 2018; 73:1059.e1017–1059.e1026.
25. Cheng S, Fang M, Cui C, et al. LGE-CMR-derived texture features reflect poor prognosis in hypertrophic cardiomyopathy patients with systolic dysfunction: preliminary results. Eur Radiol 2018; 28:4615–4624.
26. Baessler B, Luecke C, Lurz J, et al. Cardiac MRI texture analysis of T1 and T2 maps in patients with infarctlike acute myocarditis. Radiology 2018; 289:357–365.
27. Traverso A, Wee L, Dekker A, et al. Repeatability and reproducibility of radiomic features: a systematic review. Int J Radiat Oncol Biol Phys 2018; 102:1143–1158.
28. Friedman J, Hastie T, Tibshirani R. Regularization paths for generalized linear models via coordinate Descent. J Stat Softw 2010; 33:1–22.
29. Youden WJ. Index for rating diagnostic tests. Cancer 1950; 3:32–35.
30. Keren A, Goldberg S, Gottlieb S, et al. Natural history of left ventricular thrombi: their appearance and resolution in the posthospitalization period of acute myocardial infarction. J Am Coll Cardiol 1990; 15: 790–800.
31. Niemann M, Gaudron PD, Bijnens B, et al. Differentiation between fresh and old left ventricular thrombi by deformation imaging. Circ Cardiovasc Imaging 2012; 5:667–675.
32. McBride G. A proposal for strength-of-agreement criteria for Lin's concordance correlation coefficient. NIWA client report: HAM2005-062. 2005; 62.
33. Scheffel H, Baumueller S, Stolzmann P, et al. Atrial myxomas and thrombi: comparison of imaging features on CT. AJR Am J Roentgenol 2009; 192:639–645.
34. Hongo M, Okubo S, Amemiya H, et al. Diagnosis of left atrial masses by computed tomography: with special reference to the differentiation between mural thrombi and myxomas. J Cardiogr 1983; 13:935–947.
35. Abe Y, Asakura T, Sakamoto N, et al. Embolic attack in patients with atrial fibrillation and atrial thrombus depends on the character of the thrombus. Circ J 2003; 67:203–208.
36. Al-Kadi OS, Watson D. Texture analysis of aggressive and nonaggressive lung tumor CE CT images. IEEE Trans Biomed Eng 2008; 55:1822–1830.
37. Kubler D, Grafe M, Schnackenburg B, et al. T1 and T2 mapping for tissue characterization of cardiac myxoma. Int J Cardiol 2013; 169:e17–e20.
38. Caspar T, El Ghannudi S, Ohlmann P, et al. Characterization of an intracardiac melanoma metastasis by magnetic resonance T1 and T2 mapping. Int J Cardiovasc Imaging 2016; 32:1543–1544.
39. Randhawa K, Ganeshan A, Hoey ET. Magnetic resonance imaging of cardiac tumors: part 2, malignant tumors and tumor-like conditions. Curr Probl Diagn Radiol 2011; 40:169–179.
40. Konishi H, Fukuda M, Kato M, et al. Organized thrombus of the tricuspid valve mimicking valvular tumor. Ann Thorac Surg 2001; 71:2022–2024.
41. Loizou CP, Pantziaris M, Seimenis I, et al. In: Brain MR image normalization in texture analysis of multiple sclerosis. 2009 9th International Conference on Information Technology and Applications in Biomedicine: IEEE; 2009. p. 1–5.
42. Kim PK, Hong YJ, Im DJ, et al. Myocardial T1 and T2 mapping: techniques and clinical applications. Korean J Radiol 2017; 18:113–131.
43. Srichai MB, Junor C, Rodriguez LL, et al. Clinical, imaging, and pathological characteristics of left ventricular thrombus: a comparison of contrast-enhanced magnetic resonance imaging, transthoracic echocardiography, and transesophageal echocardiography with surgical or pathological validation. Am Heart J 2006; 152:75–84.